Colloids and Surfaces A: Physicochemical and Engineering Aspects 727 (2025) 138320

Contents lists available at ScienceDirect

Colloids and Surfaces A: Physicochemical and Engineering Aspects

journal homepage: www.elsevier.com/locate/colsurfa

Morphological features control drug release from nanostructured borosilicate – alginate aerogels and xerogels

Zoltán Balogh [a,b,c,*], Marcell Tátrai [a], Zoltán Dudás [c], Gergő Vecsei [d], Csaba Cserháti [d], Attila Csík [e], István Csarnovics [f], István Fábián [a], József Kalmár [a,**]

[a] HUN-REN-DE Mechanisms of Complex Homogeneous and Heterogeneous Chemical Reactions Research Group, Department of Inorganic and Analytical Chemistry, University of Debrecen, Egyetem tér 1, Debrecen H-4032, Hungary
[b] Doctoral School of Chemistry, University of Debrecen, Egyetem tér 1, Debrecen H-4032, Hungary
[c] Budapest Neutron Centre, Institute for Energy Security and Environmental Safety, HUN-REN Centre for Energy Research, Konkoly-Thege Miklós út 29-33, Budapest H-1121, Hungary
[d] Department of Solid State Physics, University of Debrecen, Bem tér 18/b, Debrecen H-4026, Hungary
[e] HUN-REN Institute for Nuclear Research (ATOMKI), Bem Tér 18/c, Debrecen H-4026, Hungary
[f] Department of Experimental Physics, Institute of Physics, Faculty of Science and Technology, University of Debrecen, Bem tér 18/a, Debrecen H-4026, Hungary

HIGHLIGHTS

- Borosilicate-alginate composite aerogels and xerogels for oral drug delivery.
- Drug impregnation during solvent-exchange, and supercritical CO_2 assisted drying.
- Different solid gel fabrication strategies yield distinct drug release properties.
- Morphological and interfacial properties are related to drug release mechanisms.

GRAPHICAL ABSTRACT

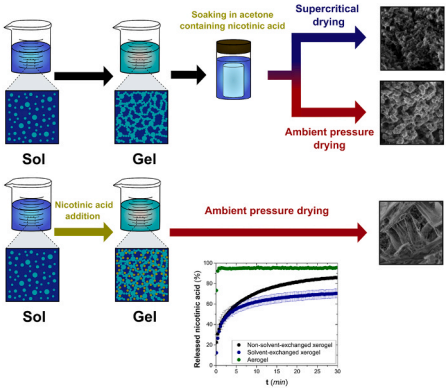

ARTICLE INFO

Keywords:
Aerogel
Xerogel
Drug delivery
Borosilicate
Alginate
Nicotinic acid

ABSTRACT

Different drug delivery systems are formulated from chemically identical borosilicate-alginate xerogels and aerogels. The backbones of these gels are prepared in a common sol-gel procedure, but the loading of the nicotinic acid drug, as well as the final drying of the impregnated wet gels were realized using different strategies. It is shown that adding the nicotinic acid during gelation and drying the wet gel under ambient conditions leads to dense xerogels with high drug loading, which is released in a moderately retarded manner in simulated gastric and intestinal fluids. Highly porous aerogels are also formulated from the identical wet gels that are impregnated with nicotinic acid post-gelation and dried using supercritical CO_2. Nicotinic acid is deposited in an

* Corresponding author at: HUN-REN-DE Mechanisms of Complex Homogeneous and Heterogeneous Chemical Reactions Research Group, Department of Inorganic and Analytical Chemistry, University of Debrecen, Egyetem tér 1, Debrecen H-4032, Hungary.
** Corresponding author.
E-mail addresses: balogh.zoltan@science.unideb.hu (Z. Balogh), kalmar.jozsef@science.unideb.hu (J. Kalmár).

https://doi.org/10.1016/j.colsurfa.2025.138320
Received 24 June 2025; Received in revised form 21 August 2025; Accepted 5 September 2025
Available online 9 September 2025

amorphous form in these aerogels, and the drug dissolves practically instantaneously in the mentioned simulated body fluids. Supercritical CO_2 drying is essential to achieve the advantageous drug solubilization feature, because drying identical gels under ambient pressure yielded xerogels that do not display burst drug release. The thorough characterization (SEM, EDS, N_2-sorption, XRD, FT-IR, Raman spectroscopy, ζ-potential) of the different gel formulations reveals the most important chemical and morphological features that control the distinct mechanisms of the release of nicotinic acid from the different gels.

1. Introduction

Aerogels and xerogels are two-phase nanostructured solids consisting of interconnected pores penetrating through a 3-dimensional skeleton. The starting point of their fabrication is the synthesis of a wet gel backbone in a liquid that initially fills their pores. Although the chemical composition and the preparation process of the gel backbone can be the same for aerogels and xerogels, they develop different final morphological features according to the drying method used to replace the pore-filling liquid with air. Xerogels are dried by evaporating the pore-filling liquid at ambient pressure, while aerogels are dried under supercritical conditions, usually using supercritical CO_2. [1–3] Supercritical drying enables the replacement of the pore-filling liquid without significant deformation of the gel backbone, because when the liquid–CO_2 mixture is taken beyond its critical point, surface tension is nullified. During ambient-pressure drying, the surface tension of the pore-filling liquid significantly deforms the original pore structure, ultimately leading to a much denser gel backbone and smaller porosity for xerogels. [4–6] Therefore, supercritically dried aerogels have characteristically higher porosities and apparent surface areas than the corresponding xerogels. [1–3] The versatility of the sol-gel method enables the production of xerogels and aerogels of various chemical compositions. [1,2,7–10] In addition to their composition, the morphological features of the gels play a crucial role in specific applications.

Aerogels and xerogels are promising functional porous materials for advanced drug delivery devices. [7,8,10] Importantly, the formulation of the final drug delivery system can be controlled in the different steps of the sol-gel preparation process, as well as by drying. The xerogels and aerogels display distinct drug delivery features, even when they have the same chemical composition. In general, aerogels facilitate rapid drug release due to their high porosity and open pore network, while xerogels typically provide prolonged drug release. [11] Besides the preparation method of the porous carrier, the technique of drug impregnation has a high impact on the delivery features. Impregnation can be realized during the sol-gel synthesis of the carrier, e.g. during the gel formation. This ensures the entrapment of a large amount of drug in the wet gel network, which has to be conserved during solvent exchange and drying for an advantageous formulation. Other typical strategies are the impregnation of the wet gel from a solution before drying (e.g. as part of solvent exchange), and the impregnation of the dry gel using supercritical CO_2. [11,12] When designing the impregnation strategy, it is essential to consider the solubility of the drug in each medium that contacts the gel, as well as, to consider the reactivity of the drug with the components of the carrier. [11]

Borosilicate glasses are being investigated as bone regenerative matrices in tissue engineering due to their tunable bioactivity and degradability. [13–15] Their backbone can be synthesized via the sol-gel method, similar to the processes used for aerogels and xerogels. [13, 15] Supercritical drying can be employed to create a highly porous structure, enhancing surface area and loading capacity. [16] The regenerative potential of these materials can be further improved by impregnating therapeutic agents into their porous networks. [14]

In our previous work, borosilicate – polyvinyl alcohol aerogels were prepared that demonstrate good biocompatibility. [16] In the present study, borosilicate–alginate hydrogels were converted into aerogels and xerogels in a similar sol-gel process. Alginates, most commonly sourced in the form of sodium alginate are intensively investigated biopolymers for hydrogel, xerogel and aerogel fabrication, because alginates are biocompatible, nontoxic, biodegradable, and show pH dependent hydration properties. [17] The combination of the biopolymer alginate with the inorganic borosilicate phase can result in a hybrid gel network with unique properties, enhancing biocompatibility and mechanical stability while providing new surface functional groups. Nicotinic acid was used as a model drug for impregnation, and testing drug release. The main objective of this research was to investigate the morphological and chemical properties of newly synthesized borosilicate–alginate aerogels and xerogels, and to determine how drying methods and different drug-loading strategies influence the drug delivery properties of these solid gels. [10,18,19] We aimed to explore the simplest alternatives for achieving satisfactory drug impregnation ratios and loadings, such as impregnation during gelation and during solvent exchange. In order to establish structure-property relationships, the chemical and the morphological characteristics of the dry gels were assessed and compared to the drug release features of the different pharmaceutical formulations. The differences in the drug release profiles were interpreted based on the structural features of the solid gel carriers taking into account the properties of the impregnated drug, as well. [20]

2. Experimental Section

2.1. Materials

Tetramethyl orthosilicate (TMOS), sodium-alginate (catalogue No. 71238; ~100 – 200 kDa MW, G/M ratio ~ 1:1) [21], ammonium fluoride, nicotinic acid (≥98 %, catalogue No. N4126), potassium chloride and monopotassium phosphate were purchased from Merck. Orto-boric acid, acetone, hydrochloric acid (37 %) and sodium dihydrogen phosphate dihydrate were obtained from VWR. Sodium chloride was purchased from Molar Chemicals Kft. The aqueous solutions were prepared with doubly-deionized and ultra-filtered water (ELGA PureLab classic system). Carbon dioxide cylinders (Biogon-C, 99.95 %) equipped with dip tube were purchased from Linde Gáz Magyarország Zrt. (Debrecen, Hungary).

2.2. Synthesis of pristine and impregnated borosilicate – alginate xero- and aerogels

The preparation steps of the aero- and xerogels are the same concerning the synthesis of the wet gel skeletons, but differ in the solvent exchange and drying processes. The impregnation of nicotinic acid is also different in the different gel formulations. The code names of the borosilicate – alginate aero- and xerogel formulations along with their preparation, and their theoretical composition are summarized in Table 1. The preparation steps are shown in Fig. 1.

The first steps of the synthesis are the same in every case. First, 6.83 mL of tetramethyl orthosilicate (TMOS) was added under gentle stirring to 4.4 mL of distilled water containing 100 μL of 0.10 M HCl. After 10 min, 30 mL of 5 w/w% aqueous boric acid, and 30 mL of 5 w/w % aqueous sodium-alginate solutions were added to the reaction mixture to ensure the homogeneous distribution of the inorganic and organic components in the final gel backbone. From this point on, the synthesis of the different gel formulations diverges, as shown in Fig. 1.

One of the possible methods for the impregnation of nicotinic acid into the gels is its introduction during the gelation step of the sol-gel

Table 1
Code names of the borosilicate–alginate aero- and xerogels, together with the different conditions used for their preparation, and their theoretical composition.

Code name	Pore-filling liquid before drying	Drying method	Drug impregnation method	Gel composition (w/w%) SiO_2 : B_2O_3 : Alginate
XS0	Native solvent	Ambient conditions	–	53: 17: 30
XSN	Native solvent	Ambient conditions	During gelation in the synthesis	53: 17: 30
AA0	Acetone	Supercritical CO_2	–	53: 17: 30
AAN	Acetone containing nicotinic acid	Supercritical CO_2	During solvent exchange	53: 17: 30
XAN	Acetone containing nicotinic acid	Ambient conditions	During solvent exchange	53: 17: 30

synthesis. In one case, after 30 min of stirring the reaction mixture, 0.90 g of nicotinic acid was directly dissolved in the mixture, and stirring was continued for another 30 min (Fig. 1**. left pathway**). Finally, 1 mL of 1.0 M NH_4F solution was added to the reaction mixture to induce gelation. The mixture was then poured into plastic molds, and gelation occurred over 24 h. To formulate drug impregnated xerogels (XSN), the monolithic gels were first cut into pieces to improve drying efficiency and reduce drying time. Finally, these pieces were dried at 50°C in a laboratory drying cabinet for 30 h. As a reference, identical xerogel without nicotinic acid (XS0) was also prepared.

For preparing other gel formulations, it has to be considered that nicotinic acid is soluble in water, as well as in acetone, but practically insoluble in supercritical CO_2. [22–24] For aerogel preparation, the pore filling water in the wet gel has to be exchanged in multiple steps to acetone. Due to its solubility in acetone, nicotinic acid can effectively be impregnated into the wet gels during such solvent exchange steps. [22–24]

Additional xerogel and aerogel formulations were prepared using the same sol-gel steps as described above until the addition of NH_4F, but without adding nicotinic acid. These wet gels were then subjected to solvent exchange and different drying methods (Fig. 1**. right pathway**). After the gelation of the original reaction mixture by NH_4F, the pristine monolithic gels were soaked in pure acetone for 24 h intervals, changing the acetone to fresh one 3 times. In the fourth step, the wet gels were soaked in 500 mL of acetone containing 1.27 g of nicotinic acid for 90 h. The impregnated wet gels were then divided into two parts, and dried using different methods (Fig. 1**. right pathway**). One part was placed in an autoclave along with the acetone solution containing nicotinic acid, and the solvated gels were dried to obtain impregnated aerogels (AAN) using supercritical CO_2 following a previously published pumpless protocol. [25] The other part of the wet gel was dried in a laboratory drying cabinet at 40°C for 7 h to produce xerogels (XAN). As a reference, aerogel without nicotinic acid (AA0) was also prepared. Photographs of the as-prepared xero- and aerogels (listed in Table 1) are shown in Fig. S1 in the Supporting Information **(SI).**

Acetone was chosen as the final solvent because the original hydrogels showed much lower shrinkage in it than in methanol or ethanol during solvent exchange. Furthermore, nicotinic acid has only moderate solubility in acetone, much lower than in the alcohols. Overall, acetone showed to be the best compromise for drug impregnation and gel drying.

2.3. Nicotinic acid content of gel formulations

Nicotinic acid is a weak acid that is highly soluble in water and has two pK_a values of 2.14 and 4.82. [26] To determine the nicotinic acid content of the impregnated dry gels, ca. 1.0 mg of powdered gel was suspended in 10 mL of HCl solution (pH = 2.0) or phosphate-buffered saline (PBS, pH = 7.4), then sonicated for 20 min, followed by stirring for ca. 20 h. After stirring, the samples were centrifuged, and the supernatant was separated. The concentration of the nicotinic acid in the supernatant was determined by UV–vis spectrophotometry with an Agilent 8453 UV–vis spectrophotometer at 261 nm (pH = 2.0) and 263 nm (pH = 7.4). The total amount of nicotinic acid was calculated based on its molar absorbance, which was determined from the calibration series recorded in each dissolution medium (see Fig. S2 in the **SI**). Based on the amount of dissolved nicotinic acid and the weight of the solid gel, the weight percentage content of nicotinic acid in the impregnated xero- and aerogels was determined.

2.4. Structural characterization

The morphological properties of the borosilicate–alginate xero- and aerogels were investigated using ***scanning electron microscopy (SEM)*** and ***N_2 adsorption-desorption porosimetry***. The chemical composition and structure of these gels were studied using ***energy dispersive X-ray spectroscopy (EDS)*** and ***Fourier-transform infrared spectroscopy (FT-IR)***. The crystalline state of the impregnated nicotinic acid was examined by ***X-ray powder diffraction (XRD)*** and ***Raman spectroscopy***. Finally, the pristine aerogel was suspended in an aqueous medium, and the ***ζ-potentials*** of the suspended aerogel microparticles were determined at different pH values using a combined dynamic light scattering (DLS) and electrophoretic mobility method. [27] The experimental procedures for sample preparation, instrumental setup, measurement protocol, and data evaluation are detailed in the electronic **SI**.

2.5. Drug release tests

The release of nicotinic acid from the impregnated xero- and aerogels was recorded using a customized fast kinetics method with on-line UV–vis spectrophotometric detection. [8,28] First, 0.50 – 1.20 mg of the powdered impregnated aerogel/xerogel was measured into a clean 1.00 cm × 1.00 cm spectrophotometric cuvette, then 3.0 mL of the dissolution medium was added to it, and UV–vis detection was immediately started. In order to simulate drug release in different organs of the human body, two dissolution media were tested: pH = 2.0 HCl and pH = 7.4 PBS solutions. The spectrum of the released nicotinic acid was recorded in the 200 – 400 nm wavelength range in every 20 s for 30 min at 37°C, with continuous stirring at 300 rpm using a 3 mm magnetic bar. The concentration of the released nicotinic acid was calculated from the on-line measured absorbance values as detailed in Section 2.3. To correct the measured absorbance of nicotinic acid for the light scattering of the gel particles, the "double-wavelength" method was applied. [29] Specifically, the absorbance values measured at 300 nm were subtracted from the absorbance values measured at 261 nm and 263 nm. The rationale is that nicotinic acid does not absorb light at 300 nm. Therefore, any increase in the absorbance at 300 nm is due to light scattering (extinction) by the gel particles. Thus, the real absorbance of nicotinic acid can be obtained by subtracting the extinction part from the measured absorbance value, as validated before. [30]

3. Results and Discussion

3.1. Nicotinic acid content of gel formulations

The nicotinic acid contents of the impregnated xero- and aerogels were determined following dissolution in different media (cf. Section 2.3), and the corresponding impregnation efficiencies are given in Table 2. The theoretical maximum nicotinic acid contents are the total amounts of nicotinic acid used for the different impregnation procedures (cf. Section 2.2).

The highest amount of nicotinic acid is present in the XSN sample,

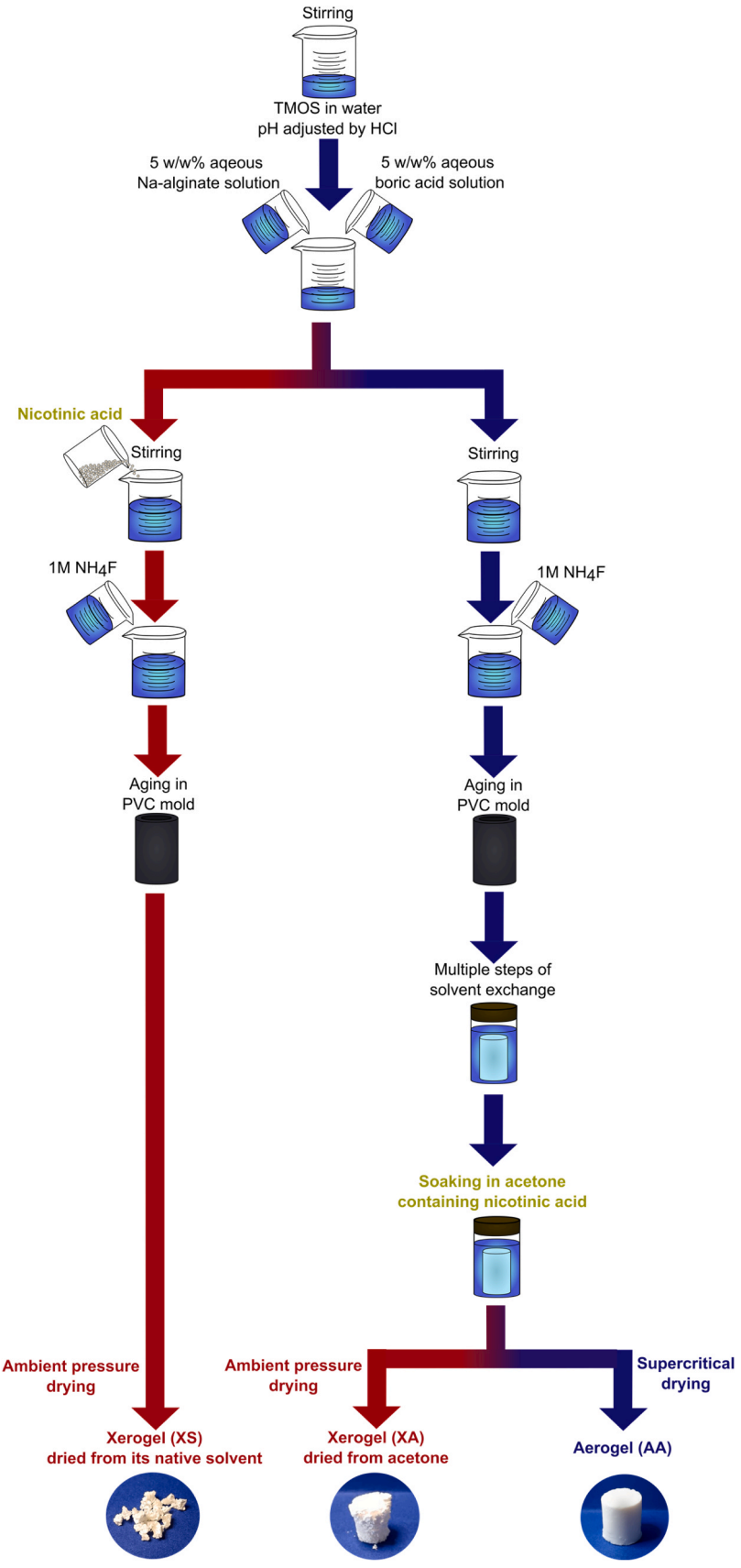

Fig. 1. Schematic representation of the preparation of pristine and impregnated borosilicate – alginate aero- and xerogels. The different pathways leading to xerogel and aerogel preparations are marked with red and blue arrows, respectively.

Table 2
The weight percentage of nicotinic acid in the impregnated gel formulations, and the corresponding impregnation efficiencies.

Sample	Nicotinic acid content (w/w)%		Impregnation efficiency
	Determined in HCl solution (pH = 2.0)	Determined in PBS (pH = 7.4)	
XSN	13.2 ± 0.1	13.5 ± 1.0	close to 100 %
AAN	3.8 ± 0.4	3.8 ± 0.3	16 %
XAN	3.3 ± 0.1	3.7 ± 0.2	16 %

while a significantly lower amount of the drug is present in XAN and AAN. Accordingly, the impregnation efficiency of XSN is close to 100 %, and much lower in the case of the XAN and AAN samples. This is rational, because nicotinic acid was directly added to the aqueous reaction mixture during the gelation step in the case of XSN, and the gel network entrapped practically the whole amount of the drug. Furthermore, no solvent exchange was performed to obtain the as-prepared XSN. For XAN, the impregnation efficiency is significantly lower, because the dissolved drug was impregnated from acetone during the solvent exchange in the already solidified wet gel skeleton. In this case, nicotinic acid spontaneously adsorbed on the gel skeleton and established an equilibrium between the solution and gel phases. This yielded a considerable amount of nicotinic acid bound to the gel network (ca. 3.7 w/w%), but still significantly less than in the case when nicotinic acid was directly added during the gelation of the carrier (cf. XSN: 13w/w% nicotinic acid). Finally, the similar nicotinic acid contents of the XAN xerogel and the AAN aerogel prove that flushing the impregnated wet gels with supercritical CO_2 does not decrease the amount of the adsorbed drug, as the only difference between the preparation of XAN and AAN is using ambient evaporation or supercritical CO_2 extraction for drying, respectively.

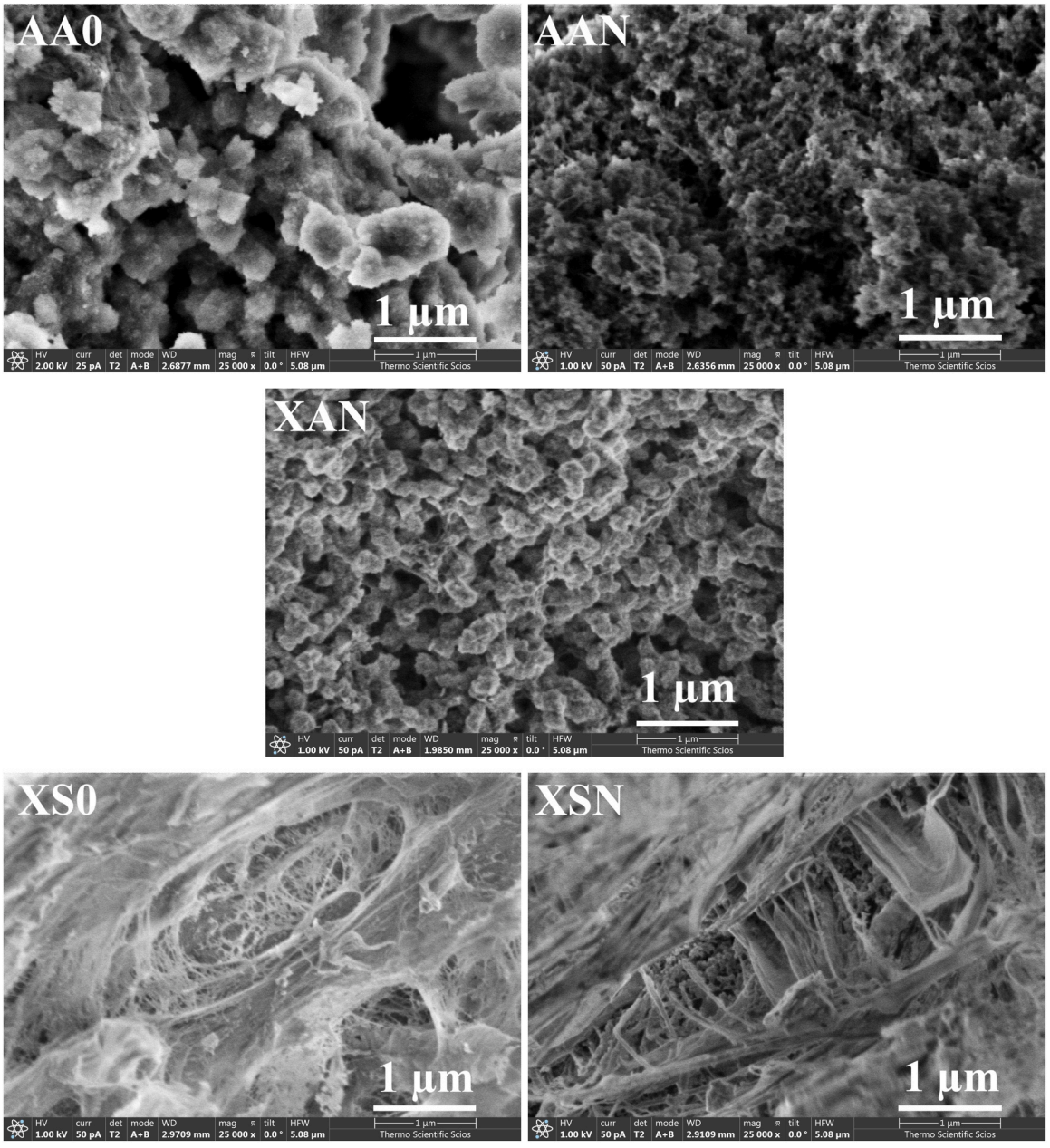

Fig. 2. Low voltage scanning electron microscopy (LV-SEM) images of pristine and impregnated borosilicate – alginate xero- and aerogels (as displayed in the legend) at 25k × magnification.

3.2. Chemical composition and morphology of gel formulations

3.2.1. Scanning electron microscopy (SEM)

Representative SEM images of the borosilicate – alginate xero- and aerogels are shown in Fig. 2**.** The AA aerogels display the fundamental morphological features of the classical silica aerogels, i.e. the backbone is built up by interconnected primary spherical nanoparticles. [16,31] However, the primary particles form large aggregates in the AA gels, and large macropores are also present in the network, which is distinct from the classical silicas. In the solvent-exchanged XA xerogels, similar morphological features are observed as in the corresponding aerogels, but a denser backbone is formed due to the shrinkage of the gel skeleton during the ambient condition drying.

Xerogels dried from their native aqueous medium (XS gels) exhibit drastically different morphological features. The spherical nanoparticles characteristic for silicas are absent, and the XS backbone is built from dense fibrillar and lamellar blocks that resemble to some extent to dry alginate gels. [21] Aggregates are also present among the fibers, which could indicate some degree of phase separation between the inorganic and organic components.

The significant morphological differences among the dry gels are the direct consequence of the interaction between the pore-filling liquid and the gel backbone during the different drying procedures. Water interacts with the hydrophilic gel backbone much stronger than acetone. During ambient pressure (open air) drying, these interactions play a significant role in determining the final morphology, because the strong capillary tension, which develops during solvent evaporation collapses the nanosized pores. These effects are stronger in the case of water (XS gels) than in the case of acetone (XA gels) due to the inherently higher surface tension of water. Furthermore, water was evaporated at moderate temperature, 50°C, to avoid thermal effects. However, this treatment took 30 h, which already induced crystallization processes leading to partial phase separation, as discussed in details later in Section 3.2.4. It was also shown that a significant amount of water still remains bound to the xerogel backbone in the XS gels, as discussed later in Section 3.2.5.

In the case of the AA aerogels, supercritical drying eliminates the deformation effects caused by capillary forces during ambient pressure drying, which explains the differences in the morphological characteristics of the AA and XA gels. It is also visible in the SEM images that the nicotinic acid containing aerogel (AAN) displays fewer macropores and a more compact skeleton than the pristine one (AA0). The presence of the relatively large amount of nicotinic acid on the surface of the gel backbone during drying may cause the noted alterations in the visible morphology.

3.2.2. N_2-sorption porosimetry

The experimental N_2-sorption isotherms and the calculated pore size distribution curves of the solvent-exchanged AA and XA gels are shown in Fig. 3. The calculated morphological parameters are collected in Table 3**.** (The skeletal densities were estimated based on literature data and the composition of the different gel formulations. [16,32]) All of these gel formulations show IVa-type (IUPAC) N_2-sorption isotherms characteristic for mesoporous materials, but the shape of the hysteresis loop is different for each. [33] The hysteresis loop for the AA0 aerogel is a combination of the H2b and H3 types, indicating the complex pore structure of the aerogel including restricted, ink-bottle shaped mesopores, together with a significant number of macropores. The impregnation of nicotinic acid into the pores has a marked effect on the apparent pore structure of the aerogel, because a typical H3 hysteresis loop is observed for AAN, which is characteristic for narrowing, wedge-shaped pores. [34] In this case, the apparent surface area decreased to approximately half of that of the pristine aerogel, and the characteristic BJH mesopore size is also reduced ca. to half. This suggests that the deposited nicotinic acid effectively narrows and blocks the mesopores, and additionally fills some of the macropores, as seen in the SEM images.

For the XAN xerogel, which was dried from acetone under ambient conditions, the hysteresis loop is H4 type due to the significant morphological changes that take place during drying due to the large capillary forces. A dramatic decrease in total pore volume and a reduction in the contribution of large pores are evident and are in good agreement with the morphological features seen in the SEM images.

N_2 adsorption-desorption porosimetry was also performed on the xerogels dried from their native solvents (XS gels); however, the measured isotherms barely exhibit a hysteresis loop, and the specific amount of adsorbed N_2 was much smaller than that for the solvent exchanged XAN xerogel. This indicates that the XS xerogels do not display mesoporosity but are built up from large bulk particles where the interparticle voids form large macropores. Thus, the apparent surface areas and pore volumes of the XS gels are outside the quantification limit of this technique.

The reason for the low porosity and low structural integrity of the XS gels is twofold. First, drying the hydrogels in open warm air causes pore collapse and extensive macroscopic shrinkage compared to the parent gel structures. As discussed already in Section 3.2.1, during the evaporation of water from the nano-sized pores, a strong capillary pressure gradient is built in the pore walls, which collapses most of the pore volume; an effect known from the literature. [35,36] Second, the high nicotinic acid content might already block most of the pores of the parent hydrogel, and during drying, the precipitating nicotinic acid can

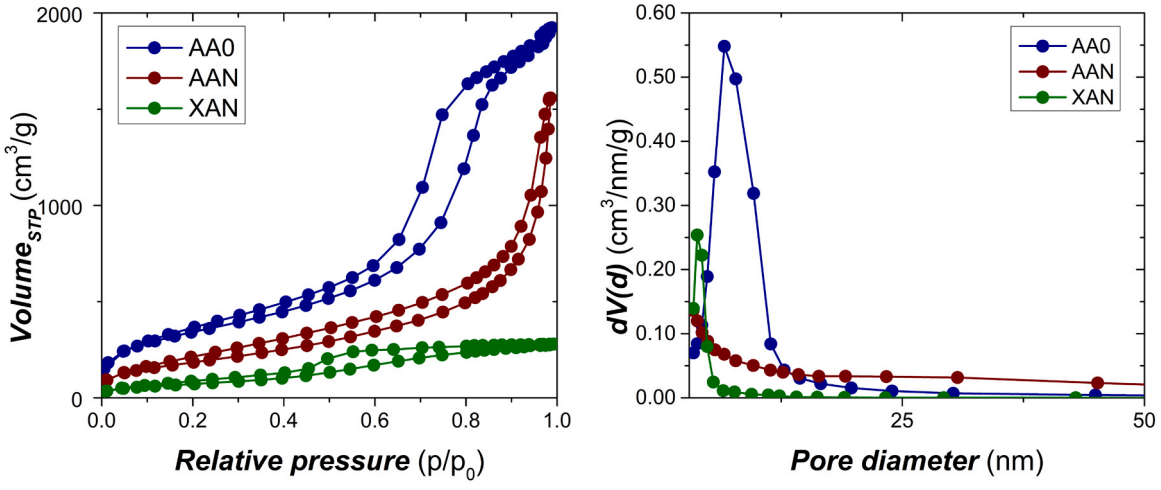

Fig. 3. Experimental N_2 adsorption-desorption isotherms (**left**) and calculated (BJH method) pore size distributions (**right**) for the different gel formulations.

Table 3
Morphological parameters of the solvent-exchanged aerogels and xerogels calculated from the N_2-sorption porosimetry results.

Sample	Bulk density	Skeletal density	Porosity[a]	BET surf. area	V_{Total}[b]	av. pore diam.[d]
	d_b [g cm^{-3}]	d_s [g cm^{-3}]	P [V/V%]	s [m^2 g^{-1}]	(BJH: $V_{3–150\ nm}$)[c] [cm^3 g^{-1}]	[nm]
AA0	0.044	2.17	98	1229	22 (3.0)	10 (72)
XS0	0.954	2.17	56	10*	0.59 (0.25*)	100* (235)
AAN	0.053	2.14	98	687	18 (2.3)	13 (107)
XAN	0.757	2.14	65	275	0.85 (0.4)	6 (12)
XSN	1.064	2.07	49	10*	0.46 (0.25*)	100* (183)

[a] Porosity calculated according to the formula: $(d_s–d_b)/d_s$, where d_s: skeletal density and d_b: bulk density.
[b] Total pore volume calculated according to formula: $1/d_b–1/d_s$.
[c] Cumulative volume of pores between 3.4 and 150 nm from N_2-sorption data and the BJH desorption method.
[d] Calculated by the 4 V/s method; V was set equal to the maximum volume of N_2 adsorbed along the isotherm as $p/p_0 \rightarrow 1.0$. For the number in parentheses, V was set equal to V_{Total} from the previous column.
* Estimated values for XS xerogels.

form thick deposits inside the xerogel structure that significantly alters the final morphology and integrity.

3.2.3. Energy dispersive X-ray spectroscopy (EDS)

Representative EDS spectra of the different gel formulations are shown in Fig. S3 in the **SI.** The elements that make up the gel backbone, namely carbon, silicon, sodium, and oxygen, which originate from the TMOS and sodium alginate precursors, can be observed in each sample. For the impregnated samples, nitrogen is also detected, further confirming the presence of nicotinic acid. In the case of the XS xerogels dried from their native solvent, boron from the boric acid precursor is also detected. Boron is difficult to detect with this technique; however, the compact structure of the XS gels together with the increased crystallinity of the backbone (*vide infra*) enhances the detection of boron. In addition to boron, aluminum appears as a contaminant in these samples, likely originating from the tools used for sample preparation.

3.2.4. X-ray powder diffraction (XRD) and Raman spectroscopy

The XRD patterns of the xero- and aerogels are shown in Figs. S4 and S5 in the **SI.** Importantly, no Bragg peaks are detectable in case of the solvent-exchanged AA and XA gels. This fact shows that both the gel skeletons, and the loaded nicotinic acid are in amorphous states in these gel formulations, which is the advantageous consequence of the use of acetone as the final solvent in their preparation procedure. The amorphous state of the nicotinic acid is an important feature that significantly influences its release from these carriers, as discussed in details in Section 3.3.

Characteristic Bragg peaks were detected in the XRD pattern of the XS0 xerogel that were assigned to crystalline boric acid derivatives. [37] Additionally, the Bragg peaks of crystalline nicotinic acid were also detected in the impregnated XSN gels. The formation of the crystalline phases in these gel formulations are the direct consequence of their ambient drying from water. This elongated (30 h) drying procedure at moderate temperature (50 °C) favored the formation of crystalline phases both in the gel backbone and in the deposited nicotinic acid.

Finally, the XRD study highlights that nicotinic acid, when introduced via impregnation from an acetone solution is deposited in an amorphous form (AAN and XAN), whereas its impregnation in the aqueous reaction mixture and subsequent ambient drying results in the crystalline drug (XSN).

In order to further study the phase of nicotinic acid in the AAN formulation, Raman spectroscopy measurements were performed. The Raman spectra of crystalline nicotinic acid, AA0 and AAN are shown in Fig. S6 in the **SI.** The bands of crystalline nicotinic acid and the gels were assigned based on literature data, as detailed in the **SI.** [38–43] As a summary, while the strong characteristic molecular vibrations of nicotinic acid are present in the Raman spectrum of AAN, the bands specifically characteristic for the crystalline form of nicotinic acid are absent. This is a further indication together with the XRD results that the nicotinic acid loaded in the AAN gel formulation does not take a crystalline form.

3.2.5. Infrared spectroscopy (IR)

The IR spectra of the xero- and aerogels, and crystalline boric acid and nicotinic acid are shown in Fig. 4**.** In general, the characteristic peaks corresponding to Si–O–Si, Si–OH, B–O, and C═O bonds, and that of the COO^- group appear in the IR spectra of solvent-exchanged XA and AA samples. The broad band observed between 3690 and 3000 cm^{-1} is attributed to the stretching vibrations of Si–OH, B–OH, and C–OH groups. [44–46] The in-plane stretching vibration of Si–O, characteristic of the Si–OH group, appears at 952 cm^{-1}. A very intense and broad band in the 1270–980 cm^{-1} range corresponds to asymmetric Si–O–Si stretching vibrations, while the symmetric stretching vibration of Si–O–Si is present at 796 cm^{-1}. [44,45] The band at 1389 cm^{-1} is assigned to the antisymmetric [BO_3] stretching vibration, whereas the peak at 663 cm^{-1} corresponds to B–O bending vibrations. [47,48] The peak near 1700 cm^{-1} is associated with the stretching vibration of the C═O bond. Additionally, the peaks at approximately 1602 cm^{-1} and 1412 cm^{-1} correspond to the asymmetric and symmetric stretching modes of the COO^- group, respectively. [45,46] An additional band at 1637 cm^{-1} is attributed to the presence of adsorbed water. [44,45] Three new peaks appear in the IR spectra of XAN at 2931 cm^{-1}, 1319 cm^{-1}, and 741 cm^{-1}. The peak at 2931 cm^{-1} corresponds to the stretching vibration of C-H bonds in nicotinic acid and alginate. [46,49] The peaks at 1319 cm^{-1} and 741 cm^{-1} correspond to the in-plane bending of the COH group in nicotinic acid and the out-of-plane bending of the COOH group in nicotinic acid, respectively. [49] The appearance of these peaks in XAN can be explained by the more compact structure of the xerogel compared to the aerogel, which enhances the detection of components present in lower concentrations.

The IR spectra of the XS xerogels dried from their native solvent show entirely different bands compared to those of the solvent-exchanged samples. In the case of XS0, the characteristic bands of boric acid are dominant, and only the characteristic silica bands are visible alongside them. In the case of the XSN, new intensive bands appear, characteristic for nicotinic acid. The difference in the spectra of the samples can be explained by their crystalline nature, as discussed in Section 3.2.4. Crystalline phases exhibit much more intensive peaks than amorphous phases; thus, crystalline boric acid and nicotinic acid contribute more significantly to the IR signal of the XS xerogels than in the case of the amorphous XA and AA gels. [45]

3.2.6. ζ-potential of suspended aerogel particles

The ζ-potential values of suspended AA0 aerogel particles are shown in Fig. S7 in the **SI** at different pH values. The calculated ζ-potential of the suspended AA0 decreases from −12 mV to −85 mV as the pH increases. In the pH range of 2.0–6.0, the ζ-potential decreases steeply, while no further decrease is observed in the pH range of 6.0–8.0. This change in the ζ-potential suggests that the surface charge of the gel particles is primarily governed by the protonation and deprotonation of

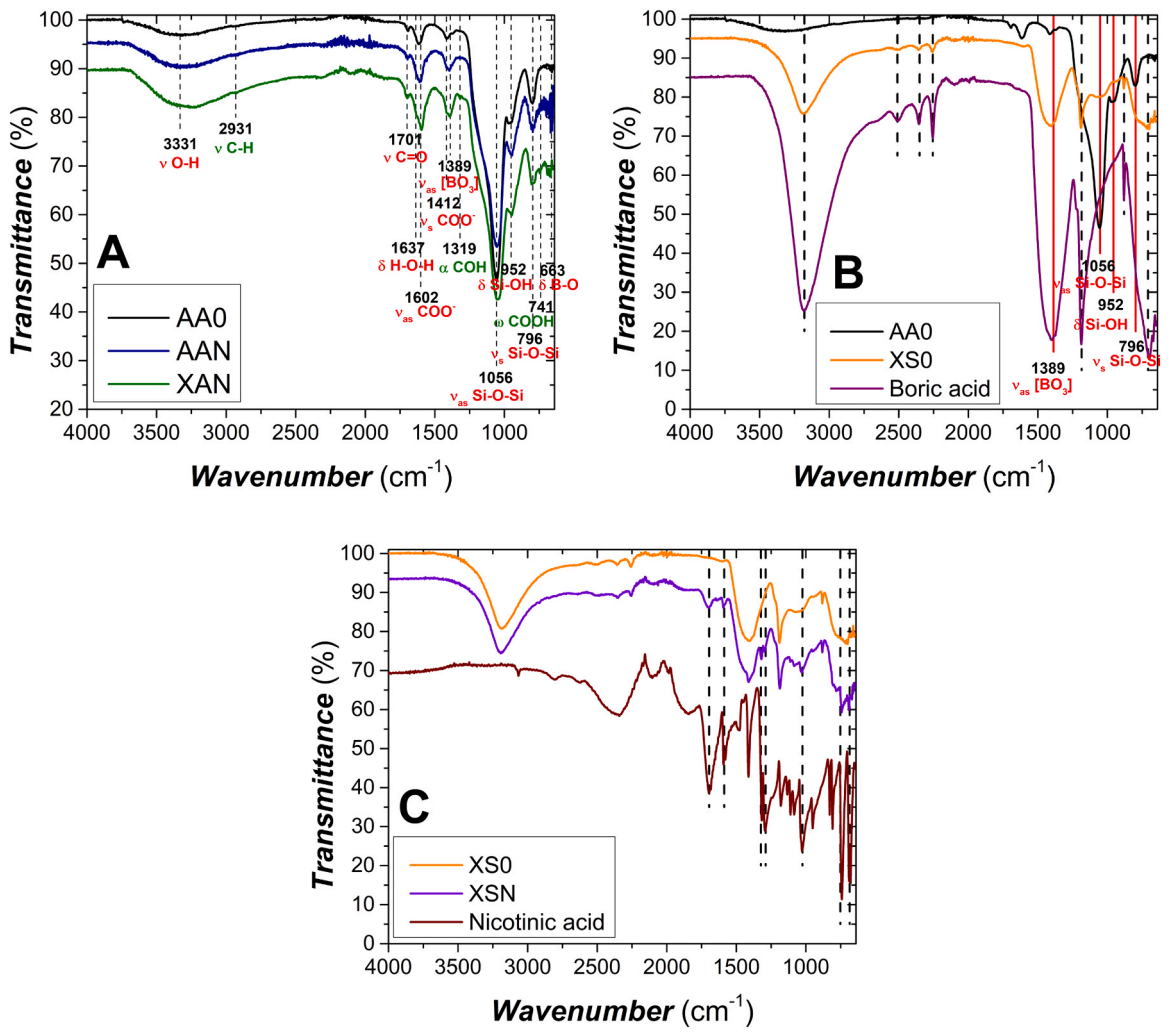

Fig. 4. Infrared spectra (FT-IR) of the different gel formulations. For reference, the spectra of crystalline boric acid and nicotinic acid are also given. The specific samples are identified in the legends. **Panel A:** IR spectra of the solvent-exchanged XA and AA gels. Peaks characteristic of different chemical bonds within the gel backbone are indicated. **Panel B**: Comparison of the IR spectra of AA0, XS0 and boric acid. Peaks characteristic of boric acid are marked with dashed lines, while those associated with the borosilicate backbone in XSN are indicated with red lines. **Panel C:** Comparison of the IR spectra of XS0, XSN and nicotinic acid. Additional peaks corresponding to crystalline nicotinic acid in the XSN sample are highlighted.

the alginate carboxyl groups that have an apparent pK_a value between 3.4 and 4.4, depending on the specific polymer structure of the studied alginate. [50]

3.3. Drug release from different gel formulations

Representative time resolved UV–vis spectra recorded during the drug release experiments (cf. Section 2.5) are shown in Fig. S8 in the **SI**. Dissolution curves representative for the different impregnated gel formulations are shown in Fig. 5. Two release profiles are shown for each formulation, i.e. total dissolved drug concentration over time, and released drug percentage over time.

Markedly the highest amount of nicotinic acid is released from the XSN xerogel at both pH = 2.0 and 7.4, which is natural since this sample has the highest nicotinic acid content (cf. Section 3.1. and Table 2). However, only the aerogel formulation is able to deploy all of the deposited drug in a quasi-instantaneous burst in less than 2 min. In the case of the xerogels, the rate of drug release is retarded compared to the aerogel formulation, and somewhat slower at pH = 7.4 than at pH = 2.0. To explain the differences in the release processes, the crystalline state of nicotinic acid, the morphological differences among the gel carriers, and the electrical charge of the components have to be taken into consideration, as follows.

Nicotinic acid is crystalline in XSN, which leads to its somewhat slower hydration and release from this xerogel. In contrast, nicotinic acid is present in an amorphous form in the other formulations, resulting in faster dissolution and release.

The instantaneous burst from the aerogel can be explained by its unique morphological features that were revealed by SEM and N_2-sorption. The aerogel has an open pore network with large macropores, allowing the entrance of the dissolution medium and the subsequent release of the hydrated drug. In contrast, xerogel samples have denser, more compact structures that hinder fluid transport in the wet gel particles. [51]

The slight pH-dependence of the drug release rate detectable in the case of the xerogel formulations can be explained by taking into account the electric charge of nicotinic acid and the gel surface. [52] Nicotinic acid has two pK_a values: 2.14 for the carboxyl group and 4.82 for the pyridine nitrogen. [26] At pH 2.0, the pyridine nitrogen is protonated and the carboxylic group is also partially protonated in equilibrium, resulting in the dominance of the zwitterionic and the cationic forms of nicotinic acid at this pH. At pH = 7.4, both groups are deprotonated, making nicotinic acid anionic. The apparent pK_a of alginic acids ranges from 3.4 to 4.4 (cf. Section 3.2.6). [50] Consequently, the carboxyl

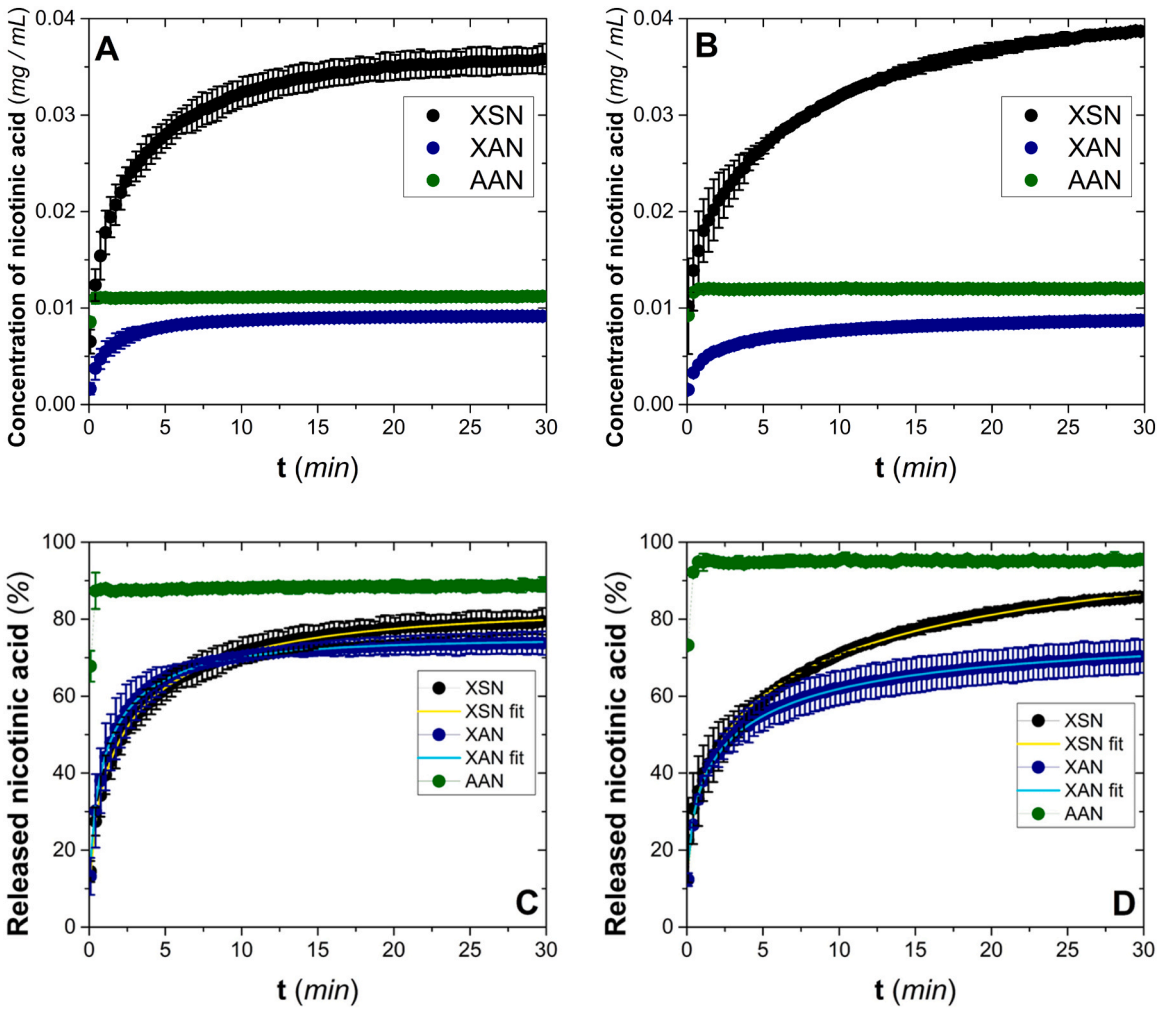

Fig. 5. Drug release from the impregnated gel formulations in different release media (cf. Section 2.5). **Top:** Concentration of nicotinic acid released from 1.00 mg impregnated gel in pH = 2.0 HCl (**A**) and in pH = 7.4 PBS (**B**). **Bottom:** Percentage of nicotinic acid released from impregnated samples in pH = 2.0 HCl (**C**) and in pH = 7.4 PBS (**D**). The continuous lines are fitted release curves using the Weibull model (Eq. 1), as explained in the main text.

groups of alginate in the gel backbone are protonated at pH = 2.0 and deprotonated at pH = 7.4 governing the ζ-potential of the surface. Thus, the faster nicotinic acid release measured at pH = 7.4 can be explained by the fact that both nicotinic acid and the gel surface are negatively charged, facilitating the fast and complete dissolution of nicotinic acid from the gels. At pH = 2.0, the surface charge of the gels is close to zero, while nicotinic acid is in its cationic and zwitterionic forms. Thus, there is no electrostatic repulsion between the components under these conditions. Another factor is the fast hydration of the solid skeleton, which is favored under both acidic and neutral conditions.

The drug release curves of the XSN and XAN formulations were fitted with the classical release models using a non-linear least-squares mathematical algorithm. The "First order", "Higuchi", "Korsmeyer-Peppas", "Hopfenberg", "Hixson-Crowell" and "Weibull" models were tested using the restrains given in the literature. [53,54] From these models, only the Weibull model (Eq. 1) gives adequate fits to the drug release curves both at pH = 2.0 and at pH = 7.4 (Fig. 5).

$$M\% = 100\ [1 - \exp(-k \times t^{n})] \quad (1)$$

In this model, M% is the accumulated fraction of drug in the release medium at time t, k is a scaling parameter analogous to a kinetic rate constant, and n is a power-law constant. As a result of the fitting procedure, $n = 0.5 \pm 0.1$ was estimated for the release curves of both XAN and XSN measured at pH = 2.0, and $n = 0.4 \pm 0.1$ was estimated for both release curves measured at pH = 7.4. These results highlight that the mechanism of drug release from the XAN and the XSN formulations is similar at both pH values, and controlled by the behavior of the gel matrices as a function of pH. Previous studies suggest that the $n = 0.4$ – 0.5 values in the Weibull model indicate that the solid gel matrices do not develop a significant hydrogel boundary layer that would restrict drug release. [55–57] The dry gels effectively hydrate and erode in both dissolution media, which enables the fast release of the loaded drug even from the xerogels. Interestingly, even the structural heterogeneity of the XSN gel has no detectable influence here. The most distinct structural properties of the xerogels (XA, XS), and the aerogel (AA) that result in distinct drug release properties is the significantly higher porosity of the aerogel, which enables the instantaneous hydration and release of drugs, while matrix erosion is needed for the liberation of nicotinic acid from both of the xerogels. (The drug release from the AAN aerogel is practically complete in the first point of the measurement at both pH values, thus modelling is not possible in these cases.)

The observations made in the drug release experiments clearly highlight the features of the different solid gel formulations. Xerogels impregnated during gelation (XSN) display a very high loading of the drug, which is released in a moderately retarded fashion both in simulated gastric (pH = 2.0) and intestinal (pH = 7.4) conditions. In contrast, aerogels impregnated after the formation of the gel skeleton (AAN) contain a significantly lower amount of drug, but in an amorphous phase, and its release is practically instantaneous in a wide pH range. Furthermore, when comparing the related XAN xerogels and AAN

aerogels, it is evident the burst release behavior of the latter is enabled by its high porosity and open mesopores, that can only be achieved by using supercritical drying as the final step of the gel preparation.

4. Conclusions

It was shown that distinctly different drug delivery systems can be formulated from a given wet gel backbone by tuning the final preparation steps in a common sol-gel procedure. Borosilicate-alginate gels of the same chemical composition were synthesized and impregnated with nicotinic acid. Both the impregnation strategies and the drying of the impregnated gels were varied to achieve different drug delivery features. The chemical and morphological characteristics of the different gel formulations were analyzed using several techniques (SEM, EDS, N_2-sorption, XRD, FT-IR, Raman spectroscopy and ζ-potential) to identify the key factors influencing the distinct release mechanisms of nicotinic acid from the various gels. Drug release from the loaded gel formulations were investigated at different pH values. When nicotinic acid is introduced during gelation, and the impregnated wet gel is dried from water under ambient conditions, the resulting xerogel displays a very high drug loading, which is released in a moderately retarded manner both in simulated gastric (pH = 2.0) and intestinal (pH = 7.4) fluids. This xerogel is characterized by a compact macroporous structure and low apparent specific surface area with a high degree of crystallinity both in the backbone and in the deposited drug. In contrast, when the same borosilicate-alginate wet gels are transferred to acetone and impregnated post-gelation, highly porous aerogels can be formulated by using supercritical CO_2 extraction for drying. The effective drug content is lower in this case, but nicotinic acid is in an amorphous form, and dissolves practically instantaneously in the common simulated body fluids. This feature enables the effective solubilization of drugs, which can be advantageous for several practical applications. It was finally shown, that supercritical drying is essential to achieve this advantageous delivery feature, because identical, but ambient condition dried xerogels do not display burst release.

CRediT authorship contribution statement

Zoltán Balogh: Writing – review & editing, Writing – original draft, Visualization, Supervision, Methodology, Investigation, Formal analysis, Data curation, Conceptualization. **Marcell Tátrai:** Writing – original draft, Visualization, Investigation, Formal analysis, Data curation. **Csaba Cserháti:** Validation, Investigation, Formal analysis, Data curation. **Attila Csík:** Validation, Investigation, Formal analysis, Data curation. **Zoltán Dudás:** Validation, Supervision, Methodology. **Gergő Vecsei:** Validation, Investigation, Formal analysis, Data curation. **István Csarnovics:** Data curation, Formal analysis, Investigation, Validation. **István Fábián:** Validation, Supervision, Resources, Methodology. **Kalmar Jozsef:** Writing – review & editing, Writing – original draft, Validation, Supervision, Resources, Methodology, Investigation, Funding acquisition, Formal analysis, Conceptualization.

Declaration of Competing Interest

The authors declare that they have no known competing financial interests or personal relationships that could have appeared to influence the work reported in this paper.

Acknowledgements

This research has been financially supported by the National Research, Development and Innovation Fund of the Ministry of Culture and Innovation, Hungary: National Research, Development and Innovation Office NKFIH NKKP SNN_150561 and EKÖP-24–3-II-DE-38 University Research Scholarship Program. This research has been financially supported by the National Research, Development and Innovation Fund of the Ministry for Innovation and Technology, Hungary (project 2019–2.1.7-ERANET-2021–00021). The research was also supported by the University of Debrecen Scientific Research Bridging Fund (DETKA) and by the University of Debrecen Program for Scientific Publication. J. Kalmár is grateful for the financial support of the János Bolyai Research Scholarship of the Hungarian Academy of Sciences.

Appendix A. Supporting information

Supplementary data associated with this article can be found in the online version at doi:10.1016/j.colsurfa.2025.138320.

Data availability

Data will be made available on request.

References

[1] H.P.S. Abdul Khalil, E.B. Yahya, H.A. Tajarudin, V. Balakrishnan, H. Nasution, Insights into the role of Biopolymer-Based xerogels in biomedical applications, Gels 8 (2022).
[2] M.A. Aegerter, N. Leventis, M. Koebel, S.A. Steiner III, Springer handbook of aerogels, Springer Nature, 2023.
[3] R. Rodríguez-Dorado, C. López-Iglesias, C.A. García-González, G. Auriemma, R. P. Aquino, P. Del Gaudio, Design of aerogels, cryogels and xerogels of alginate: effect of molecular weight, gelation conditions and drying method on Particles' micromeritics, Molecules 24 (2019).
[4] F. Shi, L. Wang, J. Liu, Synthesis and characterization of silica aerogels by a novel fast ambient pressure drying process, Mater. Lett. 60 (2006) 3718–3722.
[5] M.S. Toivonen, A. Kaskela, O.J. Rojas, E.I. Kauppinen, O. Ikkala, Ambient-Dried cellulose nanofibril aerogel membranes with high tensile strength and their use for aerosol collection and templates for transparent, flexible devices, Adv. Funct. Mater. 25 (2015) 6618–6626.
[6] J.P. Vareda, A. Lamy-Mendes, L. Durães, A reconsideration on the definition of the term aerogel based on current drying trends, Microporous Mesoporous Mater. 258 (2018) 211–216.
[7] A. Len, G. Paladini, L. Románszki, A.-M. Putz, L. Almásy, K. László, S. Bálint, A. Krajnc, M. Kriechbaum, A. Kuncser, J. Kalmár, Z. Dudás, Physicochemical characterization and drug release properties of Methyl-Substituted silica xerogels made using Sol–Gel process, Int. J. Mol. Sci. 22 (2021).
[8] P. Veres, M. Kéri, I. Bányai, I. Lázár, I. Fábián, C. Domingo, J. Kalmár, Mechanism of drug release from silica-gelatin aerogel—Relationship between matrix structure and release kinetics, Colloids Surf. B Biointerfaces 152 (2017) 229–237.
[9] D. Pércsi, A. Forgács, T. Fodor, I. Fábián, J. Kalmár, P. Herman, Nanostructured gelatin aerogel for selective recovery of aqueous Pd(II) based on coordination to the peptide backbone, ACS Appl. Nano Mater. 7 (2024) 14629–14640.
[10] A. Veronovski, Z. Novak, Ž. Knez, Synthesis and use of organic biodegradable aerogels as drug carriers, J. Biomater. Sci. Polym. Ed. 23 (2012) 873–886.
[11] C.A. García-González, A. Sosnik, J. Kalmár, I. De Marco, C. Erkey, A. Concheiro, C. Alvarez-Lorenzo, Aerogels in drug delivery: from design to application, J. Control. Release 332 (2021) 40–63.
[12] P. Gurikov, I. Smirnova, Amorphization of drugs by adsorptive precipitation from supercritical solutions: a review, J. Supercrit. Fluids 132 (2018) 105–125.
[13] D. Ishihara, A.L.B. Maçon, E. Norris, J.R. Jones, A. Obata, T. Kasuga, Borosilicate sol–gel bioactive glasses and the effect of borate content on structure-property relationships, J. Sol. Gel Sci. Technol. 114 (2025) 106–116.
[14] X. Liu, Z. Xie, C. Zhang, H. Pan, M.N. Rahaman, X. Zhang, Q. Fu, W. Huang, Bioactive borate glass scaffolds: in vitro and in vivo evaluation for use as a drug delivery system in the treatment of bone infection, Journal Materials Science Materials Medicine 21 (2010) 575–582.
[15] L. Pang, Y. Shen, H. Hu, X. Zeng, W. Huang, H. Gao, H. Wang, D. Wang, Chemically and physically cross-linked polyvinyl alcohol-borosilicate gel hybrid scaffolds for bone regeneration, Materials Science Engineering C 105 (2019) 110076.
[16] Z. Balogh, A. Len, V. Baksa, A. Krajnc, P. Herman, G. Szemán-Nagy, Z. Czigány, I. Fábián, J. Kalmár, Z. Dudás, Nanoscale structural characteristics and in vitro bioactivity of Borosilicate–Poly(vinyl alcohol) (PVA) hybrid aerogels for bone regeneration, ACS Appl. Nano Mater. 7 (2024) 4092–4102.
[17] T. Duong, M. Vivero-Lopez, I. Ardao, C. Alvarez-Lorenzo, A. Forgács, J. Kalmár, C. A. García-González, Alginate aerogels by spray gelation for enhanced pulmonary delivery and solubilization of beclomethasone dipropionate, Chem. Eng. J. 485 (2024) 149849.
[18] A.C. Hernández-González, L. Téllez-Jurado, L.M. Rodríguez-Lorenzob, SYNTHESIS OF IN-SITU SILICA-ALGINATE HYBRID HYDROGELS BY a SOL-GEL ROUTE, Carbohydr. Polym. 250 (2020) 116877.
[19] G. Horvat, M. Pantić, Ž. Knez, Z. Novak, Preparation and characterization of polysaccharide - silica hybrid aerogels, Sci. Rep. 9 (2019) 16492.
[20] Y. Li, R. Fan, H. Xing, Y. Fei, J. Cheng, L. Lu, Study on swelling and drug releasing behaviors of ibuprofen-loaded bimetallic alginate aerogel beads with pH-responsive performance, Colloids Surf. B Biointerfaces 205 (2021) 111895.

[21] A. Forgács, V. Papp, G. Paul, L. Marchese, A. Len, Z. Dudás, I. Fábián, P. Gurikov, J. Kalmár, Mechanism of hydration and hydration induced structural changes of calcium alginate aerogel, ACS Appl. Mater. Interfaces 13 (2021) 2997–3010.
[22] E.M. Gonçalves, M.E. Minas da Piedade, Solubility of nicotinic acid in water, ethanol, acetone, diethyl ether, acetonitrile, and dimethyl sulfoxide, J. Chem. Thermodyn. 47 (2012) 362–371.
[23] P. Kotnik, M. Škerget, Ž. Knez, Solubility of nicotinic acid and nicotinamide in carbon dioxide at t = (313.15 to 373.15) k and p = (5 to 30) MPa: experimental data and correlation, J. Chem. Eng. Data 56 (2011) 338–343.
[24] M. Silveira, D.A. Mayer, E.A. Rebelatto, P.H.H. Araújo, J. Vladimir Oliveira, Solubility and thermodynamic parameters of nicotinic acid in different solvents, J. Chem. Thermodyn. 184 (2023) 107084.
[25] I. Lázár, I. Fábián, A continuous extraction and pumpless supercritical CO2 drying system for Laboratory-Scale aerogel production, Gels 2 (2016).
[26] F. Gritti, G. Guiochon, Characteristics of the adsorption mechanism of acido-basic compounds with two pka in reversed-phase liquid chromatography, J. Chromatogr. A 1216 (2009) 6917–6930.
[27] C.S. Mangelsdorf, L.R. White, Electrophoretic mobility of a spherical colloidal particle in an oscillating electric field, J. Chem. Soc. Faraday Trans. 88 (1992) 3567–3581.
[28] M. Kéri, A. Forgács, V. Papp, I. Bányai, P. Veres, A. Len, Z. Dudás, I. Fábián, J. Kalmár, Gelatin content governs hydration induced structural changes in silica-gelatin hybrid aerogels – implications in drug delivery, Acta Biomater. 105 (2020) 131–145.
[29] H. Liu, J.Y. Zhu, X.S. Chai, In situ, rapid, and temporally resolved measurements of cellulase adsorption onto lignocellulosic substrates by UV−vis spectrophotometry, Langmuir 27 (2011) 272–278.
[30] T. Ditrói, J. Kalmár, J.A. Pino-Chamorro, Z. Erdei, G. Lente, I. Fábián, Construction of a multipurpose photochemical reactor with on-line spectrophotometric detection, Photochem. Photobiol. Sci. 15 (2016) 589–594.
[31] I. Lázár, A. Forgács, A. Horváth, G. Király, G. Nagy, A. Len, Z. Dudás, V. Papp, Z. Balogh, K. Moldován, L. Juhász, C. Cserháti, Z. Szántó, I. Fábián, J. Kalmár, Mechanism of hydration of biocompatible silica-casein aerogels probed by NMR and SANS reveal backbone rigidity, Appl. Surf. Sci. 531 (2020) 147232.
[32] Z. Balogh, J. Kalmár, C.J. Gommes, Wetting of alginate aerogels, from mesoporous solids to hydrogels: a small-angle scattering analysis, J. Appl. Crystallogr 57 (2024) 369–379.
[33] M. Thommes, K. Kaneko, A.V. Neimark, J.P. Olivier, F. Rodriguez-Reinoso, J. Rouquerol, K.S.W. Sing, Physisorption of gases, with special reference to the evaluation of surface area and pore size distribution (IUPAC Technical Report), 87 (2015) 1051-1069.
[34] S.S. Çok, F. Koç, A. Len, M. Kriechbaum, Z. Dudás, Antibiotic adsorption from aqueous media by using silica aerogels derived from amine-bridged silsesquioxane networks, J. Water Process Eng. 68 (2024) 106538.
[35] S. Chong, B.J. Riley, J.A. Peterson, M.J. Olszta, Z.J. Nelson, Gaseous iodine sorbents: a comparison between Ag-Loaded aerogel and xerogel scaffolds, ACS Appl. Mater. Inter 12 (2020) 26127–26136.
[36] A.C. Pierre, G.M. Pajonk, Chemistry of aerogels and their applications, Chem. Rev. 102 (2002) 4243–4265.
[37] A. Harabor, P. Rotaru, R.I. Scorei, N.A. Harabor, Non-conventional hexagonal structure for boric acid, J. Therm. Anal. Calorim. 118 (2014) 1375–1384.
[38] Y.Q. Chen, H.R. Liu, M. Zhou, The phase transition of nicotinic acid under high pressure, Vib. Spectrosc. 120 (2022) 103361.
[39] P. Koczoń, J.C. Dobrowolski, W. Lewandowski, A.P. Mazurek, Experimental and theoretical IR and Raman spectra of picolinic, nicotinic and isonicotinic acids, J. Mol. Struct. 655 (2003) 89–95.
[40] T. Furukawa, W.B. White, Raman-Spectroscopic investigation of sodium borosilicate glass structure, J. Mater. Sci. 16 (1981) 2689–2700.
[41] M. Fabian, F. Gergely, J. Osan, T. Cendak, S. Kesari, R. Rao, Structural investigation of borosilicate glasses containing lanthanide ions, Sci. Rep. 10 (2020) 7835.
[42] M. Volic, I. Pajic-Lijakovic, V. Djordjevic, Z. Knezevic-Jugovic, I. Pecinar, Z. Stevanovic-Dajic, D. Veljovic, M. Hadnadjev, B. Bugarski, Alginate/soy protein system for essential oil encapsulation with intestinal delivery, Carbohydr. Polym. 200 (2018) 15–24.
[43] I.A.D. Carmo, A.K. de Souza, L. Fayer, M. Munk, H. de Mello Brandão, L.F.C. de Oliveira, S. Bandeira, G.S. Cavallini, N.L.G.D. de Souza, Cytotoxicity and bactericidal activity of alginate/polyethylene glycol films with zinc oxide or silicon oxide nanoparticles for food packaging, Int. J. Polym. Mater. Polym. Biomater. 72 (2022) 577–588.
[44] R. Al-Oweini, H. El-Rassy, Synthesis and characterization by FTIR spectroscopy of silica aerogels prepared using several Si(OR)4 and R″Si(OR′)3 precursors, J. Mol. Struct. 919 (2009) 140–145.
[45] G. Socrates, Infrared and Raman characteristic group frequencies: tables and charts, John Wiley & Sons, 2004.
[46] R. Valentin, R. Horga, B. Bonelli, E. Garrone, F. Di Renzo, F. Quignard, FTIR spectroscopy of NH3 on acidic and ionotropic alginate aerogels, Biomacromolecules 7 (2006) 877–882.
[47] G. Shao, X. Wu, Y. Kong, S. Cui, X. Shen, C. Jiao, J. Jiao, Thermal shock behavior and infrared radiation property of integrative insulations consisting of MoSi2/borosilicate glass coating and fibrous ZrO2 ceramic substrate, Surf. Coat. Technol. 270 (2015) 154–163.
[48] J. Wan, J. Cheng, P. Lu, The coordination state of b and al of borosilicate glass by IR spectra, J. Wuhan. Univ. Technol. Mater. Sci. Ed. 23 (2008) 419–421.
[49] M. Kumar, R.A. Yadav, Experimental IR and Raman spectra and quantum chemical studies of molecular structures, conformers and vibrational characteristics of nicotinic acid and its N-oxide, Spectrochim. Acta Part A Mol. Biomol. Spectrosc. 79 (2011) 1316–1325.
[50] H. Choukaife, A.A. Doolaanea, M. Alfatama, Alginate nanoformulation: influence of process and selected variables, Pharmaceuticals 13 (2020).
[51] V. Karali, P.E. Goula, G. Patroklou, E.M. Saitani, G.E. Baltatzis, M.A. Gatou, L. C. Kontaxis, E.A. Pavlatou, S.P. Zaoutsos, I. Trougakos, G. Valsami, N. Pippa, S. Pispas, Preparation and evaluation of mixed alginate-cyclodextrin hydrogels: from physicochemical, thermotropic to swelling characterization, Colloid Surf. A 721 (2025) 137199.
[52] H. Singh, J. PonnanEttiyappan, R. BalaKrishnan, Amidated pectin and gum arabic aldehyde-based pH-sensitive hydrogel for targeted colonic treatment, Colloid Surf. A 724 (2025) 137390.
[53] P. Costa, J.M. Sousa Lobo, Modeling and comparison of dissolution profiles, Eur. J. Pharm. Sci. 13 (2001) 123–133.
[54] M. Askarizadeh, N. Esfandiari, B. Honarvar, S.A. Sajadian, A. Azdarpour, Kinetic modeling to explain the release of Medicine from drug delivery systems, Chembioeng Rev. 10 (2023) 1006–1049.
[55] V. Papadopoulou, K. Kosmidis, M. Vlachou, P. Macheras, On the use of the weibull function for the discernment of drug release mechanisms, Int. J. Pharm. 309 (2006) 44–50.
[56] M.V. Varma, A.M. Kaushal, S. Garg, Influence of micro-environmental ph on the gel layer behavior and release of a basic drug from various hydrophilic matrices, J. Control. Release 103 (2005) 499–510.
[57] B. Ecsédi, A. Forgács, Z. Balogh, I. Fábián, J. Kalmár, Hydration and wetting mechanism of borosilicate – polyvinyl alcohol (PVA) hybrid aerogels of potential bioactivity, J. Mol. Liq. 401 (2024) 124605.